PNAS RESEARCH ARTICLE | NEUROSCIENCE

Microglia regulate chandelier cell axo-axonic synaptogenesis

Nicholas B. Gallo[a,b], Artan Berisha[a], and Linda Van Aelst[a,1]

Edited by Mary Hatten, The Rockefeller University, New York, NY; received August 20, 2021; accepted January 28, 2022

Microglia have emerged as critical regulators of synapse development and circuit formation in the healthy brain. To date, examination of microglia in such processes has largely been focused on excitatory synapses. Their roles, however, in the modulation of GABAergic interneuron synapses—particularly those targeting the axon initial segment (AIS)—during development remain enigmatic. Here, we identify a synaptogenic/growth-promoting role for microglia in regulating pyramidal neuron (PyN) AIS synapse formation by chandelier cells (ChCs), a unique interneuron subtype whose axonal terminals, called cartridges, selectively target the AIS. We show that a subset of microglia contacts PyN AISs and ChC cartridges and that such tripartite interactions, which rely on the unique AIS cytoskeleton and microglial $GABA_{B1}$ receptors, are associated with increased ChC cartridge length and bouton number and AIS synaptogenesis. Conversely, microglia depletion or disease-induced aberrant microglia activation impairs the proper development and maintenance of ChC cartridges and boutons, as well as AIS synaptogenesis. These findings unveil key roles for homeostatic, AIS-associated microglia in regulating proper ChC axonal morphogenesis and synaptic connectivity in the neocortex.

microglia | axon initial segment | chandelier cells | synaptogenesis | inflammation

Significance

Chandelier cells (ChCs) are a unique type of GABAergic interneuron that form axo-axonic synapses exclusively on the axon initial segment (AIS) of neocortical pyramidal neurons (PyNs), allowing them to exert powerful yet precise control over PyN firing and population output. The importance of proper ChC function is further underscored by the association of ChC connectivity defects with various neurological conditions. Despite this, the cellular mechanisms governing ChC axo-axonic synapse formation remain poorly understood. Here, we identify microglia as key regulators of ChC axonal morphogenesis and AIS synaptogenesis, and show that disease-induced aberrant microglial activation perturbs proper ChC synaptic development/connectivity in the neocortex. In doing so, such findings highlight the therapeutic potential of manipulating microglia to ensure proper brain wiring.

The proper development and function of cortical networks is reliant on the postnatal establishment and maintenance of synaptic connections between diverse neural cell populations. While synapse development and plasticity are well known to be finely regulated by neuron–neuron interactions (1–3), increasing studies have begun to elucidate the participation of glial cells, such as microglia and astrocytes, in shaping the synaptic landscape in the developing central nervous system (CNS) (4–7). In particular, microglia, the resident macrophages of the CNS, are becoming increasingly appreciated as dynamic regulators of synaptic connectivity (8–11).

While microglia have traditionally been viewed as central to inflammatory and phagocytic responses to pathogens, cellular debris, and neural injury, new roles for microglia under normal, physiological conditions have begun to emerge over recent years (8, 11–13). Mounting evidence indicates that microglia leverage their phagocytic activity to remove extranumerary or inappropriate synapses/synaptic material in the developing CNS, a process critical for sculpting the precise, organized neural circuitry found in the adult brain (14–17). Interestingly, in addition to their phagocytic activities, microglia have more recently been recognized as key regulators of synapse development, function, and plasticity (8, 12, 18–24). For example, microglia were found to promote dendritic spine formation via the induction of spine head filopodia in the hippocampus and somatosensory cortex (SSC) and regulate different forms of synaptic plasticity in distinct brain regions (12, 21, 22). These newly appreciated functions, though, have primarily been studied in the context of microglia-excitatory pyramidal neuron (PyN)/principal cell interactions. To date, surprisingly little is known about microglia-GABAergic interneuron bidirectional communication in the developing brain.

In contrast to excitatory PyN–PyN synapses, which typically form on dendritic spine protrusions, GABAergic interneurons form inhibitory synapses onto various targeted PyN subcellular domains, including the dendritic shaft, cell body, and axon initial segment (AIS) (25). Microglia have recently been reported to make direct contact with PyN somas and are implicated in the pruning and stripping/displacement of axo-somatic presynaptic terminals during development and following inflammation, injury, or complex febrile seizures, respectively (26–29). Whether microglia also play a synaptogenic role, though, in the regulation of axo-somatic synapses in the developing brain warrants further investigation. In addition, very little to nothing is known about the involvement of microglia in regulating dendrite-targeting, and particularly AIS-targeting, GABAergic interneuron synapse formation, and remodeling under either physiological or pathological conditions.

A unique type of GABAergic interneuron that forms axo-axonic synapses exclusively onto the AIS of PyNs are chandelier cells (ChCs) (30–33). These cells, which

Author affiliations: [a]Division of Neuroscience, Cold Spring Harbor Laboratory, Cold Spring Harbor, NY 11724; and [b]Department of Neurobiology and Behavior, Stony Brook University, Stony Brook, NY 11794

Author contributions: N.B.G. and L.V.A. designed research; N.B.G. and A.B. performed research; N.B.G. and A.B. analyzed data; and N.B.G. and L.V.A. wrote the paper.

The authors declare no competing interest.

This article is a PNAS Direct Submission.

See online for related content such as Commentaries.

[1]To whom correspondence may be addressed. Email: vanaelst@cshl.edu.

This article contains supporting information online at http://www.pnas.org/lookup/suppl/doi:10.1073/pnas.2114476119/-/DCSupplemental.

Published March 9, 2022.

predominantly derive from progenitors in the ventral medial ganglionic eminence during late gestation, possess a distinctive, highly branched axon that terminates in multiple parallel arrays of short, vertically oriented terminals of presynaptic boutons, called cartridges (34–36). Each of these cartridges selectively innervates neighboring PyN AISs, the site of action potential initiation, enabling ChCs to exert decisive control over PyN firing and population output (30, 32, 33, 37–39). Developmental profiling revealed that ChC axons undergo dramatic arborization/branching and AIS synapse formation starting at approximately postnatal day 11/12 (P11/12) before reaching final maturity by the end of the fourth postnatal week in mice (40–42). At this time, most PyN AISs in layers 2/3 (L2/3) of the SSC are selectively innervated by three to four ChC cartridges deriving from distinct ChCs (40, 43). The mechanisms, though, governing ChC connectivity/axo-axonic synapse formation still remain poorly understood. Recent studies have begun to identify ChC-expressed molecules—including ErbB4, DOCK7, FGF13, and IgSF11, and PyN-expressed L1CAM—as key components essential for proper ChC cartridge/bouton development and ChC/PyN AIS innervation, respectively (40, 44–48). The roles, however, of extrinsic cues and other cell types in regulating ChC axonal morphogenesis and axo-axonic synapse formation are completely unknown.

In this study, we focused on the roles of microglia in tripartite microglia–PyN AIS–ChC interactions under both physiological and pathological conditions. We found that such interactions are dependent on an intact, ankyrin-G (AnkG)/βIV-spectrin–expressing PyN AIS cytoskeleton and microglial $GABA_{B1}$ receptors ($GABA_{B1}$Rs), and are associated with a marked increase in ChC cartridge length and bouton number and AIS synaptogenesis in the postnatal developing neocortex. Conversely, depletion of microglia impaired the proper formation and maintenance of ChC cartridges/boutons, as well as ChC/PyN AIS GABAergic synapse formation, supporting a synaptogenic function for homeostatic microglia in proper ChC/PyN axo-axonic synaptogenesis in the healthy brain. In line with this, we found that AIS GABAergic synapse density was considerably reduced when microglia were activated under lipopolysaccharide (LPS)-induced, acute neuroinflammatory conditions and in a transgenic mouse model of Alzheimer's disease (AD). Together, our findings shed new light on the roles of microglia in GABAergic interneuron development/synaptogenesis and identify microglia as the only glial cell type known to date to regulate neocortical ChC axonal morphogenesis and synaptic connectivity.

Results

Increased Cytoskeletal-Dependent Microglia–PyN AIS Contacts Coincide with the Early Phase of Neocortical ChC Axonal Development and AIS Synaptogenesis. To assess whether microglia regulate neocortical ChC axo-axonic synapse formation, we began by investigating microglia interactions with the postsynaptic site of ChC/PyN synaptic innervation: namely, the AIS, at P14 when the length of PyN AISs is at its longest and ChC axonal morphogenesis and AIS synaptic innervation rapidly begin to develop (40, 49, 50) (Fig. 1*D*). Murine brain sections were coimmunostained for AnkG and Iba1 to label AISs and microglia, respectively. Analysis of microglia–AIS interactions in L2/3 of the SSC at P14 revealed a notable fraction (~14%) of $Iba1^+$ microglia, hereafter referred to as AXIS (axon initial segment-associated) microglia, that intimately associate with the AIS of PyNs (Fig. 1 *A*–*C*). In line with a previous report (51), we found such microglia closely wrap at least one of their processes around an AIS, typically descending down the AIS from the microglia soma, which directly opposes the PyN cell body (Fig. 1*A*). The orientation/directionality of AXIS microglia–AIS associations appear variable though, as AXIS microglia processes were also observed ascending the AIS or emanating bidirectionally from an AXIS microglia positioned in the middle of the AIS (*SI Appendix*, Fig. S1*A*). These observations suggest potential functions for microglia–AIS interactions during early postnatal development, especially as ChC/PyN axo-axonic synapses are first being formed.

To corroborate and extend these findings, we profiled microglia–AIS interactions from P8 to adulthood (2 to 3 mo of age) in L2/3 of the murine SSC. We found that the number of AXIS microglia–PyN AIS contacts was relatively low at the end of the first postnatal week (~8% at P8) prior to the onset of extensive ChC axonal elaboration and ChC/PyN AIS innervation (40), but doubled within the next 4 d, peaking at ~15% from P12 to P28 (black line in Fig. 1*D*) when dynamic ChC axonal morphogenesis and PyN AIS innervation and associated GABAergic transmission are occurring (40, 41) (dotted blue line in Fig. 1*D*). The majority of both AXIS and non-AXIS microglia during the second/third postnatal week were ramified in shape (Fig. 1*A* and *SI Appendix*, Fig. S1*B*). Analysis in adulthood showed that PyN AIS–AXIS microglia associations dropped back to baseline levels (~8%), with AXIS, and also non-AXIS, microglia maintaining their typical ramified structure (Fig. 1*D* and *SI Appendix*, Fig. S1*C*). This temporal pattern of microglia–PyN AIS contact was mirrored by the number of microglia present in L2/3 of the SSC (*SI Appendix*, Fig. S1*D*). These results identify a distinct temporal window during the second/third postnatal week of murine SSC development when PyN AIS–AXIS microglia associations are most prevalent, which remarkably coincides with the rapid onset of ChC axonal development, synaptogenesis, and GABAergic signaling (40, 41).

Since proper AIS synaptic innervation by ChCs is dependent on the unique AIS cytoskeleton (40), we next examined whether AXIS positioning of microglia is similarly reliant on a structurally intact AIS. We performed RNA interference (RNAi)-mediated knockdowns of the AIS-enriched cytoskeletal/scaffolding proteins AnkG, βIV-spectrin, and PSD-93 in L2/3 PyNs in the SSC (Fig. 1 *E*–*G* and *SI Appendix*, Fig. S1 *E* and *F*) (49, 50, 52). Given that AXIS microglia numbers, as well as ChC/PyN AIS innervation, start to spike by the end of the second postnatal week, analyses of the percentage of electroporated GFP^+ and neighboring GFP^- (internal control) PyN AISs contacted by AXIS microglia were performed at P14. In line with previous work (51), we found that PyN knockdown of AnkG, the master organizer of the AIS (49, 50), substantially reduced the percentage of GFP^+ PyNs with AXIS microglia at P14 relative to both control RNAi conditions and nonelectroporated, AnkG-expressing PyNs in the same brain hemisphere/field-of-view (Fig. 1 *F* and *G*). Moreover, depletion of PyN-expressed βIV-spectrin, which links AnkG to actin rings in the AIS (49, 50) and, like AnkG, is required for ChC/PyN AIS innervation (40), also significantly decreased the percentage of electroporated PyNs contacted by AXIS microglia (Fig. 1 *F* and *G*). On the other hand, knockdown of the scaffolding protein PSD-93, which was shown to be enriched at cortical PyN AISs (52) but not required for ChC/PyN AIS innervation, did not impact the percentage of PSD-93–depleted PyNs contacted by AXIS microglia (Fig. 1 *F* and *G*). Of note, knockdown of any of these molecules in PyNs did not affect microglia numbers (*SI Appendix*, Fig. S1*F*). These findings demonstrate the requirement of an intact AnkG/βIV-spectrin–expressing PyN AIS in facilitating AXIS microglia–PyN AIS interactions during early postnatal development.

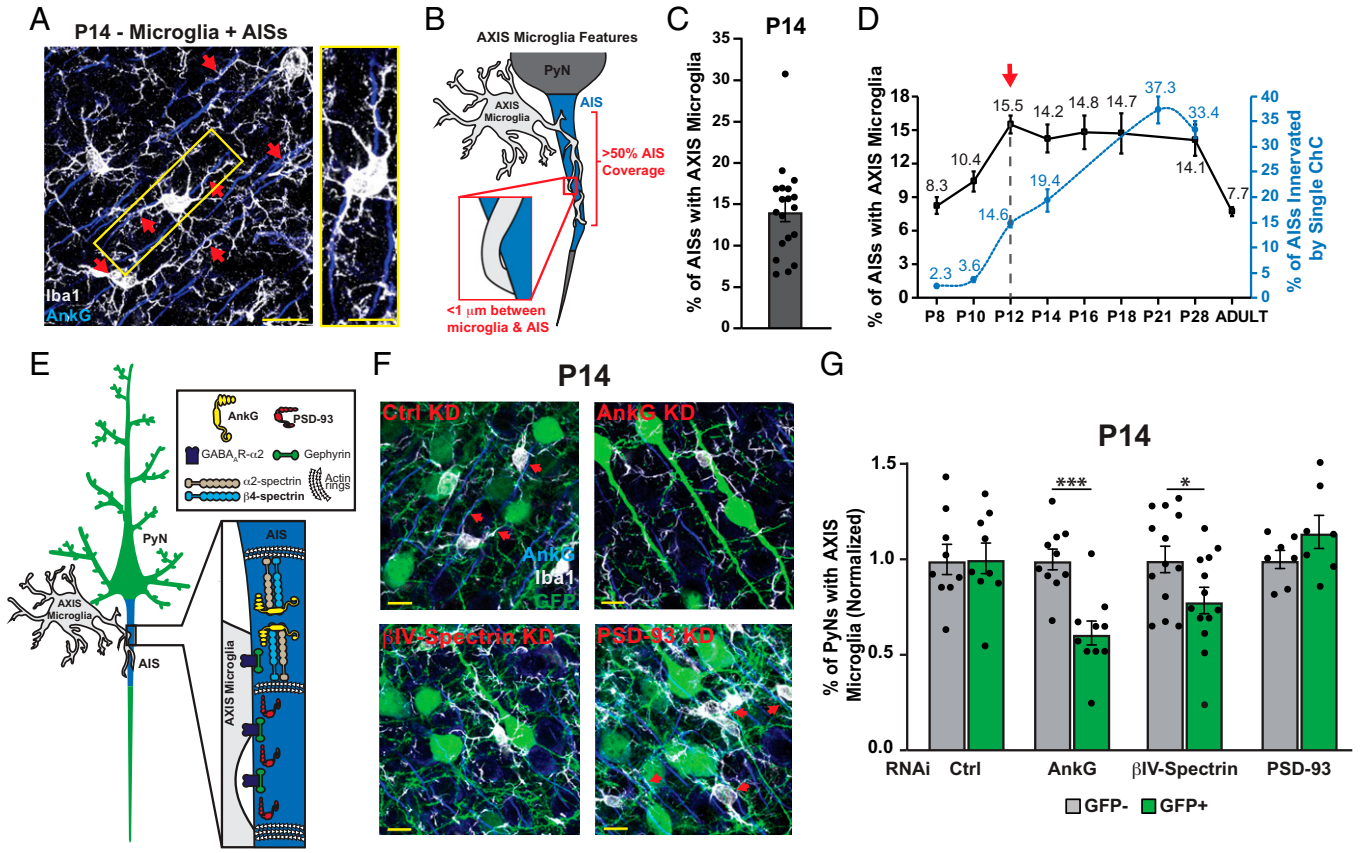

Fig. 1. AIS cytoskeleton-dependent enrichment of AXIS microglia in the neocortex between P12 and P28. (*A*) Immunofluorescent labeling of Iba1$^+$ microglia and AnkG$^+$ AISs in L2/3 of the SSC in wild-type mice at P14. (Scale bars, 10 μm.) Arrows in *A* and *F* depict AXIS microglia–PyN AIS contact. (*B*) Schematic depicting the two key morphological features of AXIS microglia: 1) at least 50% microglial coverage of AIS length and 2) <1 μm distance between microglia and AIS surface. (*C*) Quantification of the percentage of PyN AISs contacted by AXIS microglia at P14. (*D*) Quantification of the percentage of AISs contacted by AXIS microglia (black line) and percentage of AISs innervated by single, labeled ChCs (dotted blue line) at time points spanning P8 to adulthood in L2/3 of the SSC. Dashed gray line and red arrow denote spike in the percentage of AISs with AXIS microglia and AISs innervated by ChCs starting at P12. (*E*) Schematic depicting cytoskeletal components and GABA$_A$Rs at PyN AISs. (*F*) Representative images of GFP$^+$ (green) and neighboring GFP$^-$ PyNs and AnkG$^+$ AISs (blue) with or without Iba1$^+$ AXIS microglia (white) contact in L2/3 of the SSC from P14 mice electroporated at E15.5 with vectors coexpressing EGFP and short-hairpin RNAs targeting AnkG, βIV-spectrin, PSD-93, or control firefly luciferase (Ctrl). (Scale bars, 10 μm.) (*G*) Quantification of the percentage of GFP$^+$ and neighboring GFP$^-$ PyN AISs contacted by AXIS microglia. Data are mean ± SEM, *P < 0.05, ***P < 0.001 (Student's t tests); n values and statistical information are listed in *SI Appendix*, Table S1.

Tripartite AXIS Microglia–PyN AIS–ChC Interactions Are Associated with Increased ChC Cartridge Length and Bouton Number in the Postnatal Developing Neocortex. Our above findings raise the possibility that PyN AIS–AXIS microglia interactions could play a role during early postnatal morphogenesis of AIS-targeting ChCs and in ChC/PyN AIS synapse formation. To address this, we investigated whether AXIS microglia–PyN AIS–ChC tripartite interactions correlate with aspects of presynaptic ChC cartridge/bouton and axo-axonic synapse development. We performed Iba1 and AnkG coimmunostainings of brain sections from *Nkx2.1-CreER;Ai9* mice, in which ChCs are sparsely labeled with the fluorescent marker RFP (35), ranging in age from P8 to adulthood. Confocal imaging revealed a marked increase in the number of AIS-innervating ChC axon terminals intimately contacted by microglial processes between the second to third postnatal week (Fig. 2 *A–C*). Indeed, the percentage of ChC cartridges contacted by microglia at the AIS increased nearly 25% from P12 to P14–16 before dropping back to baseline levels by adulthood (Fig. 2*D*).

Interestingly, we found AIS-innervating ChC cartridges juxtaposed to AXIS microglia had an increased length and number of boutons per cartridge on average relative to AIS-innervating ChC cartridges lacking AXIS microglia contact. This positive correlation was observed from P12 to P18, coinciding with the developmental time frame when AXIS microglia numbers and tripartite interactions, ChC axonal morphogenesis, and ChC/PyN AIS innervation first spike in L2/3 of the SSC (Fig. 2 *E–H* and *SI Appendix*, Fig. S4*A*) (40). By the end of the fourth postnatal week and into adulthood, average ChC cartridge length and bouton number per cartridge were comparable between cartridges with and without AXIS microglia contact, likely indicating the final maturation of such synaptic structures (Fig. 2 *G* and *H*). These data point toward a growth-promoting/synaptogenic role for microglia in microglia–PyN AIS–ChC interactions during the second/third week of postnatal development.

Of note, in line with a synaptogenic (rather than a phagocytic) function of microglia on ChCs during this time window, analysis of ChC engulfment by microglia in L2/3 of the SSC found only 3 of 120 Iba1$^+$ microglia analyzed contained RFP$^+$ ChC inclusions between P12 and P28 (*SI Appendix*, Fig. S2 *A–C*). In accordance with this, analysis of microglial CD68 puncta, an indicator of microglia activation/phagocytosis (53), found comparable puncta numbers between AXIS and non-AXIS microglia (*SI Appendix*, Fig. S2 *D* and *E*). As a positive control for microglial phagocytosis and to rule out any possible detection issues arising from the quenching of internalized RFP$^+$ material, analysis of ChC engulfment by microglia was performed at the V1/V2L border region at

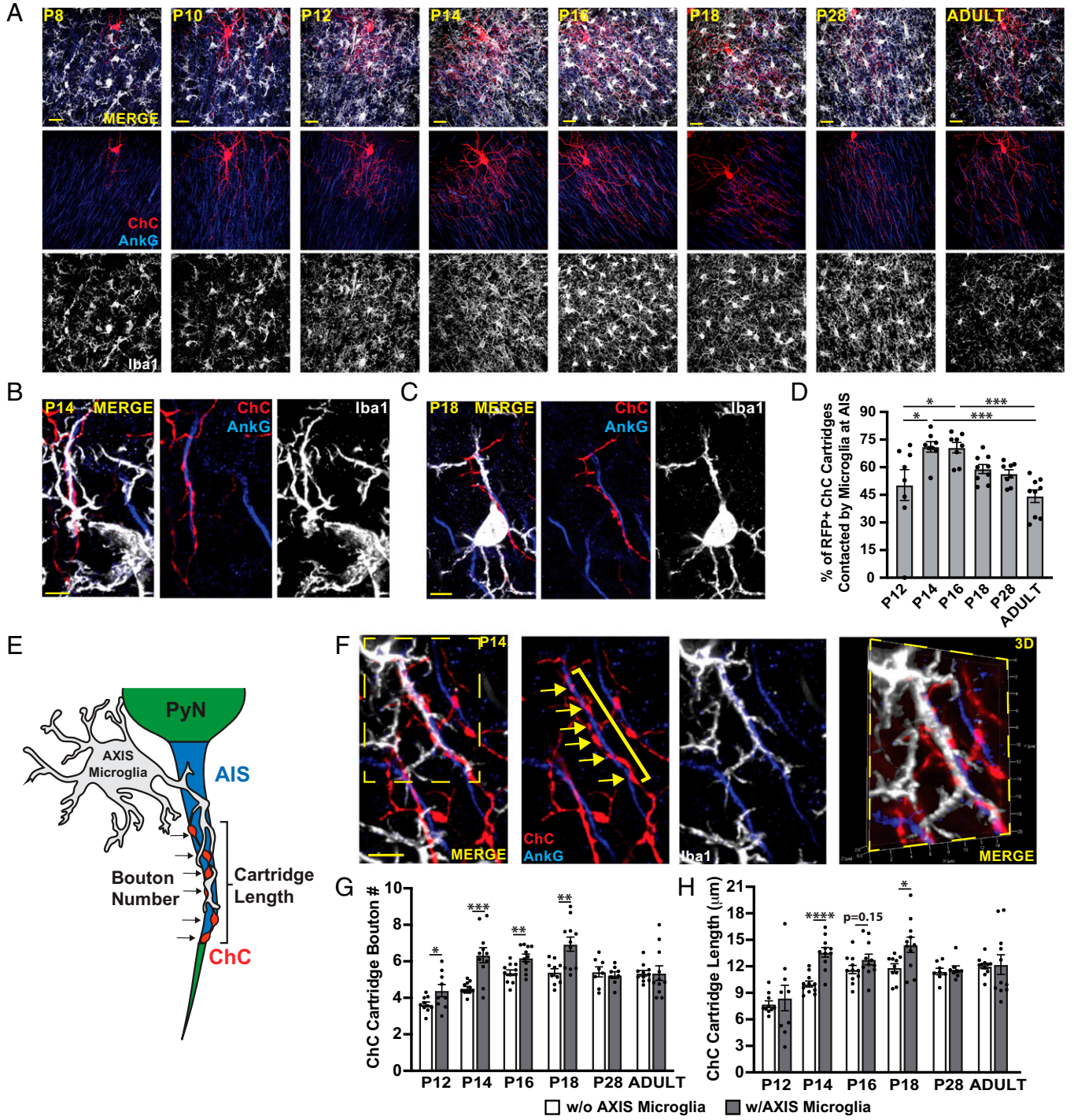

Fig. 2. Microglia–PyN AIS–ChC cartridge tripartite interactions are associated with increased ChC cartridge length and bouton number during postnatal development. (*A*) Immunofluorescent labeling of Iba1$^+$ microglia, AnkG$^+$ AISs, and RFP$^+$ ChCs in L2/3 of the SSC in *Nkx2.1-CreER;Ai9* mice at indicated time points. (Scale bars, 20 μm.) (*B* and *C*) Representative images of Iba1$^+$ AXIS microglia–AnkG$^+$ PyN AIS-RFP$^+$ ChC cartridge tripartite interactions at P14 (*B*) and P18 (*C*). (Scale bars, 5 μm.) (*D*) Quantification of the percentage of RFP$^+$ cartridges from a single ChC contacted by microglia at the AIS in L2/3 of the SSC. (*E*) Schematic of AXIS microglia–PyN AIS–ChC interactions with arrows denoting individual boutons of a single ChC cartridge and bracket denoting ChC cartridge length. (*F*) Representative image of RFP$^+$ ChC cartridge–PyN AIS innervation with AXIS microglia contact in L2/3 of the SSC at P14. (Scale bar, 5 μm.) Three-dimensional representation of dashed boxed region is included (*Right*). (*G* and *H*) Quantification of the average number of boutons per ChC cartridge (*G*) and the average length of ChC cartridges (*H*) innervating AISs with or without AXIS microglia contact at indicated time points. Data are mean ± SEM, $*P < 0.05$, $**P < 0.01$, $***P < 0.001$, $****P < 0.0001$ (one-way ANOVA with post hoc Tukey's multiple comparison test in *D*; Student's *t* tests in *G* and *H*); *n* values and statistical information are listed in *SI Appendix*, Table S1.

P10, when ChCs are undergoing activity-dependent cell death and their cellular debris must be removed (54). In this paradigm, internalized RFP$^+$ ChC material was frequently observed, indicating that RFP$^+$ fragments could be detected after being engulfed by microglia (*SI Appendix*, Fig. S2 *F* and *G*). These results indicate that, unlike at the murine V1/V2L border region at P10, microglia do not regularly phagocytose ChC material in L2/3 of the SSC during early postnatal development.

Altogether, these results support a growth-promoting/synaptogenic role for microglia in tripartite microglia–PyN AIS–ChC interactions during early postnatal neocortical development.

Microglia Play a Key Role in ChC Cartridge/Bouton Development and AIS Synaptogenesis. To determine whether microglia directly contribute to ChC axon terminal development and synapse formation, we depleted microglia in *Nkx2.1-CreER;Ai9* mice with PLX3397 (PLX), a CSF1R/c-kit antagonist commonly used to reduce microglia numbers (17, 55), via daily oral gavage from P7 to P14 or P18. Brains from PLX- or vehicle-treated animals were collected on the last day of treatment, sectioned, and coimmunostained for AnkG and Iba1, and analyzed for ChC cartridge length and bouton number per cartridge. In addition, separate brain slices were coimmunostained for AnkG, Iba1, and gephyrin, a postsynaptic marker of GABAergic synapses, to visualize and quantify the density of gephyrin^{+} puncta at PyN AISs (i.e., axo-axonic ChC/PyN synapses). Notably, microglial depletion in the SSC via PLX was observed as early as 3 d after the onset of treatment (*SI Appendix*, Fig. S3*A*), with nearly 100% of microglia ablated by P14 and P18 (Fig. 3 *A* and *G* and *SI Appendix*, Fig. S3 *B, C, F,* and *G*). PLX administration did not perturb ChC/PyN AIS percent innervation nor induce off-target ChC innervation at PyN somas (*SI Appendix*, Fig. S3 *D, E, H,* and *I*). In addition, no change in cortical astrocyte numbers nor major gross morphological alterations of ChCs, PyNs, or PyN AIS structure were observed in the SSC under PLX-treated conditions (Fig. 3 *A* and *G* and *SI Appendix*, Fig. S3 *J–S*).

Consistent with a growth-promoting role for microglia, we found that the average length and bouton number of ChC cartridges were significantly decreased when microglia were depleted from P7 to P14 (Fig. 3 *B–D*) and P7 to P18 (Fig. 3 *H–J*), relative to vehicle-treated, AXIS microglia conditions and, interestingly, were similar to the fraction of AIS-innervating ChC cartridges lacking AIS microglia contact under physiological conditions (*SI Appendix*, Fig. S4 *B* and *C*). Such a decrease was also apparent when ChC cartridge bouton number and length were plotted as frequency distribution histograms, which revealed a larger fraction of short ChC cartridges with fewer boutons under both microglia depletion paradigms (Fig. 3 *Cii*, *Dii*, *Iii*, and *Jii*). Furthermore, we observed a significant reduction in gephyrin puncta density at PyN AISs under PLX conditions relative to control PyN AISs ensheathed by AXIS microglia (Fig. 3 *E*, *F*, *K*, and *L*). To corroborate these findings and ensure the above results were not due to PLX-induced c-kit inhibition, we performed similar analysis in *Csf1r* knockout (KO) mice, which lack microglia throughout the brain but maintain proper AIS number and structure (*SI Appendix*, Fig. S5 *A–D*) (56). Such analysis also revealed a significant decrease in gephyrin puncta density at PyN AISs in L2/3 of the SSC relative to control PyN AISs ensheathed by AXIS microglia in wild-type mice (*SI Appendix*, Fig. S5 *E* and *F*). Combined, these data identify microglia as key cellular players facilitating/promoting ChC cartridge/bouton morpho- and synaptogenesis during early postnatal development.

Microglia Are Important for Maintaining the Integrity of ChC Cartridges/Boutons. We next asked whether microglia are also involved in the maintenance of ChC cartridges/boutons and axo-axonic synapses in adulthood. Given that mature ChC morphology and ChC/PyN connectivity are largely attained by the end of the first postnatal month (40), we administered PLX to *Nkx2.1-CreER;Ai9* mice from P48 to P58 to deplete microglia after ChC/PyN circuitry was already established. PLX-mediated reduction in microglia number in L2/3 of the SSC was confirmed via Iba1 immunostaining (Fig. 4*A* and *SI Appendix*, Fig. S6). No gross morphological alterations of PyNs or ChCs were observed under PLX-treated conditions (Fig. 4 *A* and *B*). Interestingly, we found that both ChC cartridge length and bouton number per cartridge were slightly, but significantly, reduced under PLX conditions at P58 relative to ChC cartridges contacted by AXIS microglia under control conditions (Fig. 4 *B–D*). In line with this, gephyrin puncta density at PyN AISs was significantly reduced in PLX-treated animals, suggesting a contributive role for microglia in maintaining ChC/PyN AIS synaptic connectivity (Fig. 4 *E* and *F*). These data indicate that under physiological conditions, microglia are not only important for proper ChC axon terminal morphogenesis and synaptogenesis during the establishment of neocortical ChC/PyN AIS connectivity but also for the maintenance of ChC cartridge/bouton integrity in adulthood.

Depletion of Microglial $GABA_{B1}$ Receptors Impacts Microglia–PyN AIS Interactions and ChC Synaptogenesis. Our above findings raise the question as to what molecular processes facilitate tripartite AXIS microglia–PyN AIS–ChC interactions. Our present data show that while homeostatic AXIS microglia are important for proper ChC–AIS synaptogenesis, they are not required for the establishment of ChC/PyN AIS contacts. We previously identified PyN-expressed L1CAM as a critical cell adhesion molecule (CAM) required for innervation of neocortical PyN AISs by ChCs (40). On the other hand, previous work has shown that GABAergic signaling regulates synaptic pruning and synaptogenesis while also inducing chemical, morphological, and electrical responses in $GABA_BR$-expressing microglia (57–63). Along these lines, microglial expression of $GABA_BRs$ was found to increase between embryonic and postnatal stages (58, 60, 61) and, interestingly, $GABA_{B1}R$ removal from microglia was recently reported to selectively impact inhibitory connectivity (29). Based on these findings, we postulated that L1CAM-mediated ChC/PyN AIS initial contact and subsequent GABAergic neurotransmission recruit microglia to the AIS through microglial sensing of GABA via their expression of $GABA_{B1}Rs$.

To test this hypothesis, we first verified by immunohistochemistry the expression of $GABA_{B1}Rs$ in microglia in L2/3 of the SSC of wild-type animals and, importantly, demonstrated that AXIS microglia express $GABA_{B1}Rs$ (*SI Appendix*, Fig. S7). We then generated conditional mutant mice lacking $GABA_{B1}Rs$ in microglia using the *Cx3cr1-Cre*-driver mouse line (cKO, *Cx3cr1-Cre;*$GABA_{B1}R^{fl/fl}$), as described previously (29), and examined the impact of microglial $GABA_{B1}R$ ablation on AXIS microglia–PyN AIS interactions and ChC/PyN AIS synaptogenesis. We found that the percentage of PyN AISs contacted by AXIS microglia was significantly decreased in L2/3 of the SSC of P18 cKO mice and, importantly, also observed a significant reduction in AIS gephyrin puncta density (Fig. 5 *A–D*). Of note, removal of $GABA_{B1}Rs$ from microglia did not affect total microglia numbers (Fig. 5*E*). In sum, these data unveil a critical role for microglial $GABA_{B1}Rs$ in facilitating microglia–PyN AIS interactions and ChC/PyN AIS synaptogenesis, and together with our above findings, further support a specific function for microglia in the observed ChC synaptogenic phenotype.

Microglia Activation under Neuroinflammatory Conditions Perturbs ChC Cartridge/Bouton Development and Synaptogenesis. It is by now well-appreciated that microglia have diverse functional responses during physiological and neuroinflammatory/pathological conditions. For example, in response to an injury/insult, microglia become activated and shift into different functional states, modifying their proliferation, morphology,

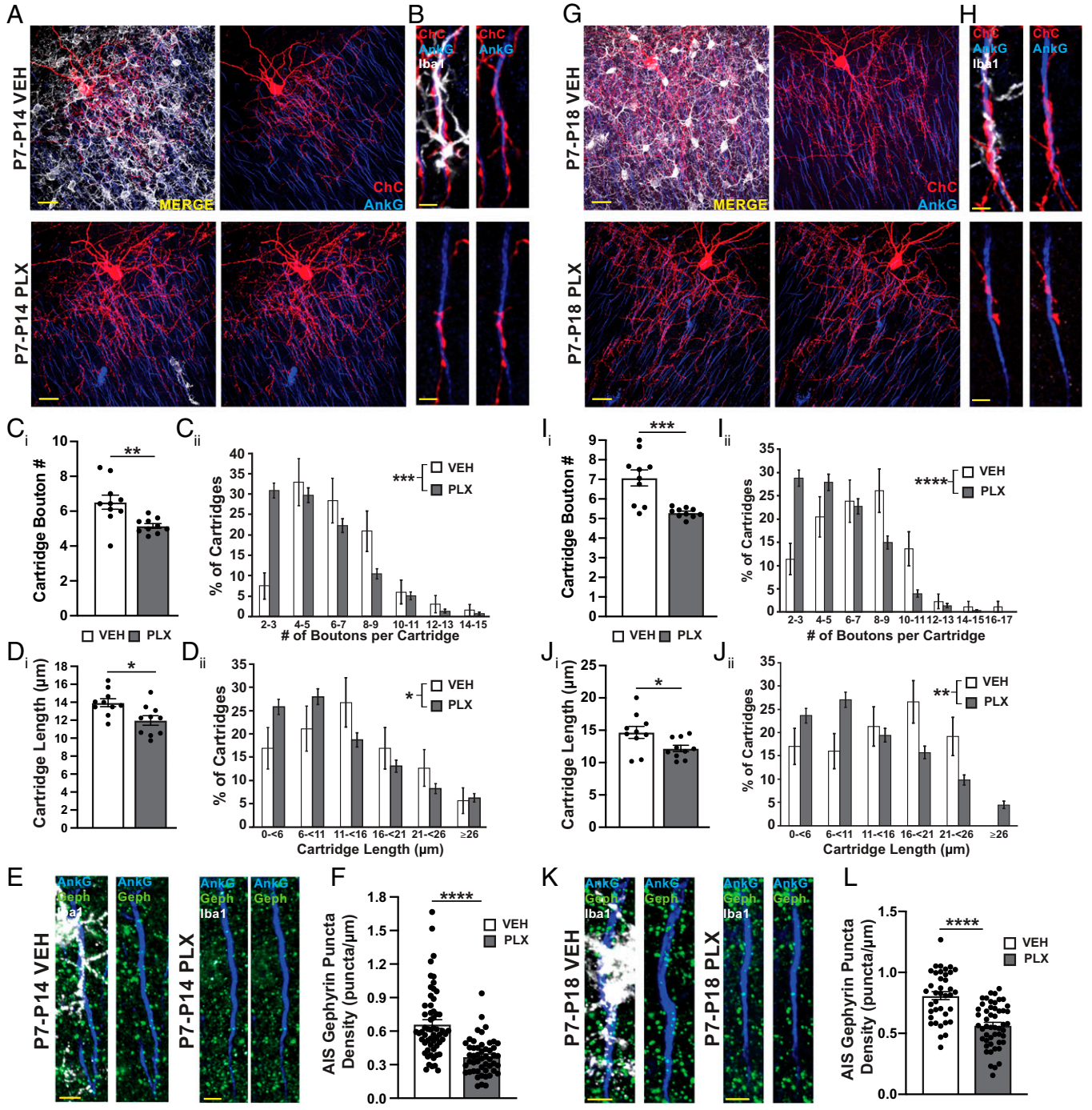

Fig. 3. Early postnatal depletion of microglia impairs neocortical ChC cartridge/bouton development and AIS synaptogenesis. (*A* and *G*) Representative images of single RFP$^+$ ChCs, neighboring AnkG$^+$ AISs, and Iba1$^+$ microglia in L2/3 of the SSC from P14 (*A*) or P18 (*G*) *Nkx2.1-CreER;Ai9* mice administered PLX or vehicle once daily from P7 to P14 (*A*) or P18 (*G*). (Scale bars, 20 μm.) (*B* and *H*) Representative images of RFP$^+$ ChC cartridge–PyN AIS innervation with or without AXIS microglia contact from P14 (*B*) or P18 (*H*) *Nkx2.1-CreER;Ai9* mice under PLX or vehicle conditions. (Scale bars, 3 μm.) (C_i, D_i, I_i, and J_i) Quantification of the average number of boutons per ChC cartridge (C_i and I_i) and the average length of ChC cartridges (D_i and J_i) innervating PyN AISs with or without AXIS microglia contact at P14 (C_i and D_i) or P18 (I_i and J_i) in the SSC of *Nkx2.1-CreER;Ai9* mice under PLX or vehicle conditions. (C_{ii}, D_{ii}, I_{ii}, and J_{ii}) Frequency distribution histograms showing the percentage of ChC cartridges with bouton number per cartridge ranging from 2 to 17 boutons (C_{ii} and I_{ii}) and cartridge length ranging from 0 to ≥26 μm (D_{ii} and J_{ii}) with or without AXIS microglia contact at P14 (C_{ii} and D_{ii}) or P18 (I_{ii} and J_{ii}) under PLX or vehicle conditions. (*E* and *K*) Representative images of PyN AISs with or without AXIS microglia contact in L2/3 of the SSC from P14 and P18 mice treated with PLX or vehicle from P7 to P14 (*E*) or P18 (*K*). GABAergic synapses are visualized by immunostaining for gephyrin (Geph). (Scale bars, 3 μm.) (*F* and *L*) Quantification of average gephyrin puncta density at AISs with or without AXIS microglia contact at P14 (*F*) or P18 (*L*). For C_i, D_i, I_i, J_i, *F*, and *L*, data are mean ± SEM. For C_{ii}, D_{ii}, I_{ii}, and J_{ii}, error bars indicate SEM for a multinomial distribution. *$P < 0.05$, **$P < 0.01$, ***$P < 0.001$, ****$P < 0.0001$ (Student's *t* tests in C_i, D_i, I_i, J_i, *F*, and *L*; two-tailed Mann–Whitney *U* tests in C_{ii}, D_{ii}, I_{ii}, and J_{ii}); *n* values and statistical information are listed in *SI Appendix*, Table S1.

phagocytic activity, antigen presentation, and the release of factors, such as cytokines, chemokines, and repulsive guidance molecules (8, 64–66). This prompted us to investigate the effects of microglia activation on ChC cartridge/bouton development and synaptogenesis under pathological conditions. We reasoned that disease-induced perturbations in microglial homeostasis would hinder normal ChC development in a manner similar to our depletion studies when homeostatic microglia are absent. We first

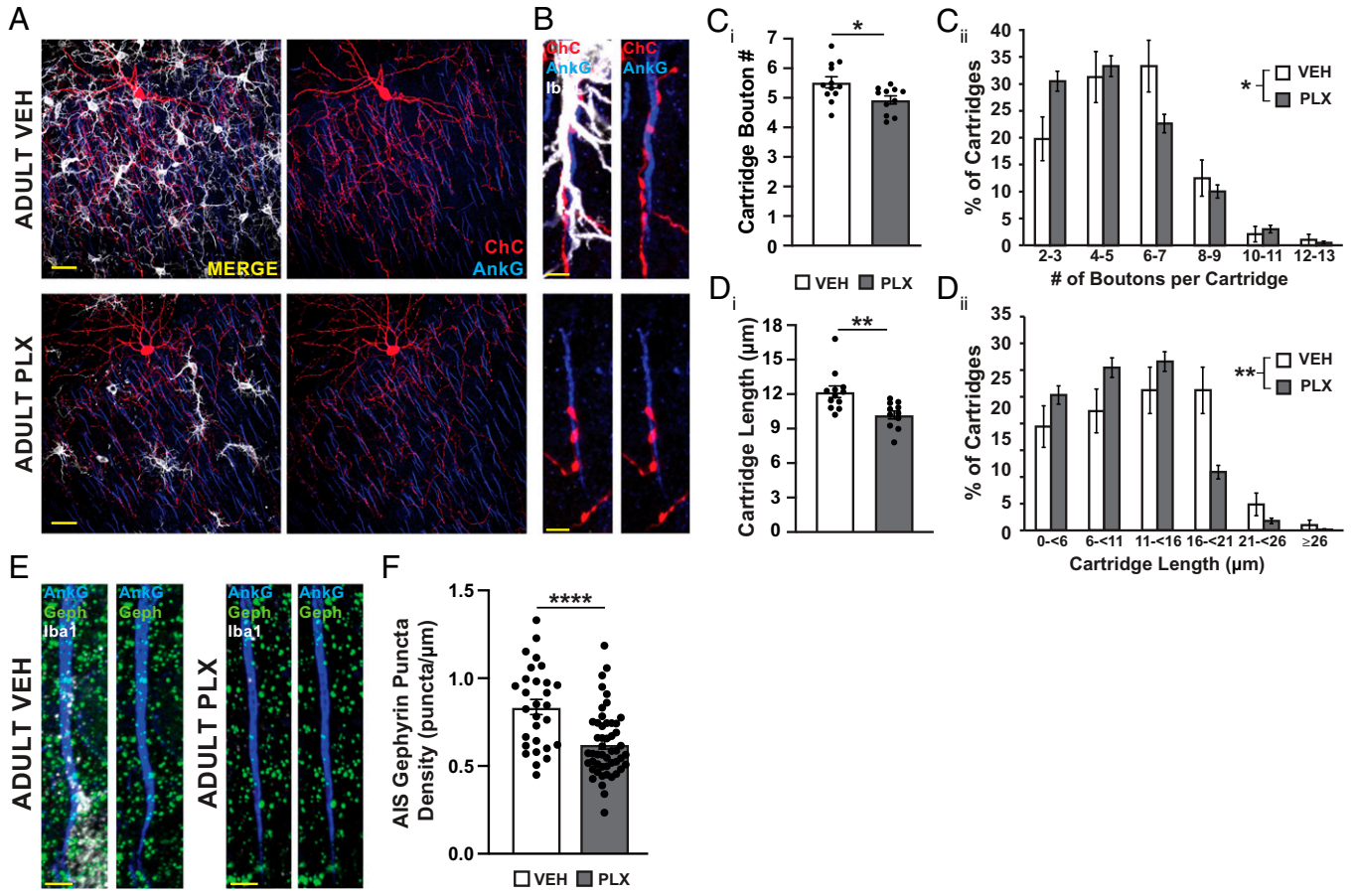

Fig. 4. Microglia are important for the maintenance of neocortical ChC cartridges/boutons. (*A*) Representative images of single RFP$^+$ ChCs, neighboring AnkG$^+$ AISs, and Iba1$^+$ microglia in L2/3 of the SSC from P58 *Nkx2.1-CreER;Ai9* mice administered PLX or vehicle once daily from P48 to P58. (Scale bars, 20 µm.) (*B*) Representative images of RFP$^+$ ChC cartridge–PyN AIS innervation with or without AXIS microglia contact from P58 *Nkx2.1-CreER;Ai9* mice under PLX or vehicle conditions. (Scale bars, 3 µm.) (C_i and D_i) Quantification of the average number of boutons per ChC cartridge (C_i) and average length of ChC cartridges (D_i) innervating PyN AISs with or without AXIS microglia contact at P58 in the SSC of *Nkx2.1-CreER;Ai9* mice under PLX or vehicle conditions. (C_{ii} and D_{ii}) Frequency distribution histograms showing the percentage of ChC cartridges with bouton number per cartridge ranging from 2 to 13 boutons (C_{ii}) and cartridge length ranging from 0 to ≥26 µm (D_{ii}) with or without AXIS microglia contact at P58 under PLX or vehicle conditions. (*E*) Representative images of PyN AISs with or without AXIS microglia contact in L2/3 of the SSC from P58 mice treated with PLX or vehicle from P48 to P58. GABAergic synapses are visualized by immunostaining for gephyrin (Geph). (Scale bars, 3 µm.) (*F*) Quantification of average gephyrin puncta density at AISs with or without AXIS microglia contact at P58. For C_i, D_i, and *F*, data are mean ± SEM. For C_{ii} and D_{ii}, error bars indicate SEM for a multinomial distribution. *$P < 0.05$, **$P < 0.01$, ****$P < 0.0001$ (Student's *t* tests in C_i, D_i, and *F*; two-tailed Mann–Whitney *U* tests in C_{ii} and D_{ii}); *n* values and statistical information are listed in *SI Appendix*, Table S1.

resorted to the commonly used LPS-induced model of neuroinflammation, in which administration of LPS, an endotoxin derived from the outer membrane of gram-negative bacteria, causes rapid and robust microglia activation in the CNS (27). LPS or PBS vehicle was injected intraperitoneally once daily in *Nkx2.1-CreER;Ai9* mice from P12 to P15 and ChC cartridge length and bouton number per cartridge were analyzed at P16. LPS administration substantially changed microglia morphology and increased CD68 puncta number per microglia, indicating their robust activation (M_{LPS} classification), and increased total microglia numbers and the percentage of PyN AISs with AXIS microglia in L2/3 of the SSC (Fig. 6 *A*–*C* and *SI Appendix*, Fig. S8 *A*–*D*). On the other hand, no gross morphological alterations of ChCs, PyNs, or PyN AIS structure were observed (Fig. 6 *A* and *B* and *SI Appendix*, Fig. S8 *E*–*G*).

Subsequent analysis revealed a significant reduction in ChC cartridge length and bouton number per cartridge under acute, inflammatory LPS conditions relative to control (Fig. 6 *Ai*, *Bii*, *D*, and *E*). Quantification of AIS gephyrin puncta density also revealed a significant reduction in axo-axonic synapses at PyN AISs contacted by M_{LPS} AXIS microglia (Fig. 6 *F* and *G*). Intriguingly, analysis of engulfment of RFP$^+$ ChC material by microglia under LPS- and vehicle-treated conditions found no significant evidence of ChC phagocytosis, with only one instance of engulfment in 45 M_{LPS} microglia and zero engulfments in 45 vehicle-treated microglia observed (*SI Appendix*, Fig. S8 *H*–*J*), suggesting that distinct mechanisms are responsible for the observed decrease in axo-axonic synapse formation. In this regard, LPS has been reported to trigger the release of cytokines that can antagonize the effects of synaptogenic factors released by microglia (9, 67). Interestingly, unlike early LPS administration, induction of acute LPS-mediated neuroinflammation in adulthood (*SI Appendix*, Fig. S9*A*) did not significantly perturb the average length and bouton number of M_{LPS} AXIS microglia-associated ChC cartridges nor AIS gephyrin puncta density (*SI Appendix*, Fig. S9 *F*–*I*), despite inducing a marked change in microglia morphology as well as a small increase in total microglia numbers and the percentage of PyN AISs with AXIS microglia (*SI Appendix*, Fig. S9 *B*–*E*). As expected, no evidence of microglial engulfment of RFP$^+$ ChC material nor any changes in PyN or ChC gross morphology were observed in adulthood under LPS-treated conditions (*SI Appendix*, Fig. S9 *E* and *J*–*L*).

Altogether, these data demonstrate that acute, LPS-mediated activation of microglia specifically during the critical time

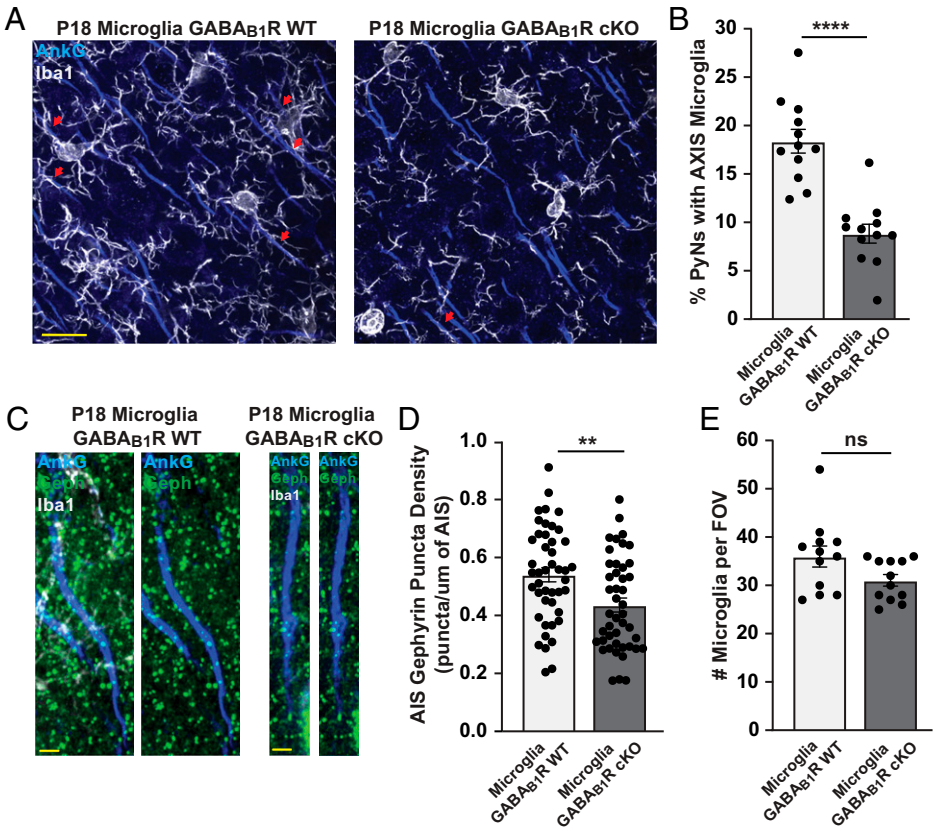

Fig. 5. Removal of $GABA_{B1}$Rs from microglia impacts AXIS microglia numbers and AIS GABAergic synaptogenesis. (*A*) Representative images of Iba1$^+$ microglia and AnkG$^+$ AISs in L2/3 of the SSC from P18 *Cx3cr1-Cre;GABA$_{B1}$R$^{fl/fl}$* (microglia $GABA_{B1}$R cKO) and wild-type littermates. Arrows denote AXIS microglia-PyN AIS contact. (Scale bar, 15 μm.) (*B*) Quantification of the percentage of PyN AISs contacted by AXIS microglia in P18 microglia $GABA_{B1}$R cKO and wild-type mice. (*C*) Representative images of PyN AISs with or without AXIS microglia contact in L2/3 of the SSC from P18 microglia $GABA_{B1}$R cKO and wild-type mice. GABAergic synapses are visualized by immunostaining for gephyrin (Geph). (Scale bars, 2 μm.) (*D* and *E*) Quantification of average AIS gephyrin puncta density (*D*) and average microglia number per 200 μm × 200 μm field-of-view (FOV) (*E*) in P18 microglia $GABA_{B1}$R cKO and wild-type mice. For *B*, *D*, and *E*, data are mean ± SEM, $^{**}P < 0.01$, $^{****}P < 0.0001$, ns (not significant) indicates $P \geq 0.05$ (Student's *t* tests); *n* values and statistical information are listed in *SI Appendix*, Table S1.

window of initial ChC cartridge/bouton morphogenesis and synaptogenesis hinders these developmental processes, while acute, LPS-induced microglia activation in adulthood after ChC/PyN circuits have formed does not apparently affect the integrity of established ChC cartridges/boutons.

AD-Associated *β*-Amyloid Plaque Formation Increases AXIS Microglia Numbers and Reduces AIS GABAergic Synapse Density in the Neocortex. While acute, LPS-induced microglial activation in adulthood did not significantly impact established ChC cartridges/boutons, we questioned whether chronic neuroinflammation, which is a hallmark of AD (66, 68), impacts axo-axonic synapse density at PyN AISs. To test this, we took advantage of the AD *APPswe,PSEN1de9* (hereafter referred to as AβPP/PS1) transgenic mouse model, which is characterized by a steadily increasing amyloid-β (Aβ) plaque load starting at approximately 6 to 7 mo of age (69). Analysis of AβPP/PS1 animals at 14 mo of age, several months after the initial appearance of plaques and neuroinflammation, revealed a heavy plaque burden in the neocortex (Fig. 6*H* and *SI Appendix*, Fig. S10 *A* and *B*), with microglia number almost doubling in L2/3 of the SSC and displaying altered morphology, indicative of an activated state (Fig. 6 *H* and *I*). Besides apparent contact between PyN AISs and Aβ plaques, we found that the percentage of PyNs with AXIS microglia increased more than fourfold relative to control animals (Fig. 6*J* and *SI Appendix*, Fig. S10*C*).

Next, we investigated whether this change in the percentage of PyN AISs with activated AXIS microglia impacted ChC/PyN AIS synapse numbers by quantifying AIS gephyrin puncta density in 14-mo-old AβPP/PS1 and control littermates. Such analyses revealed a significant reduction in the density of gephyrin$^+$ synapses at PyN AISs contacted by AXIS microglia under AD conditions (Fig. 6 *K* and *L*). Of note, PyN AIS structure was still morphologically intact in 14-mo-old AβPP/PS1 animals (*SI Appendix*, Fig. S10 *C–F*). We also assessed ChC/PyN AIS synapses in such animals by quantifying AIS puncta density of the presynaptic GABAergic synapse marker VGAT. Such analyses revealed a similar phenotype, with VGAT puncta density significantly decreased at PyN AISs contacted by activated, AXIS microglia in AβPP/PS1 animals (*SI Appendix*, Fig. S10 *G* and *H*). It is worth noting that similar AIS gephyrin and VGAT puncta density were observed between AXIS microglia-contacted AISs in 14-mo-old control animals and AISs lacking activated AXIS microglia contact in 14-mo-old AβPP/PS1 mice, implying that the reduction in AIS GABAergic synapses in the AβPP/PS1 model is likely a result of activated microglia contact and not a global phenomenon found throughout the AD brain (Fig. 6*L* and *SI Appendix*, Fig. S10*H*). Together, these findings indicate that chronic, AD-induced pathology and associated microglial activation in adulthood significantly impacts ChC/PyN synaptic connectivity. They also further reinforce the importance of homeostatic microglia in regulating GABAergic AIS synapses throughout the entire lifespan, potentially helping to explain the growing number of reports linking perturbed excitatory/inhibitory balance and microglia dysfunction to AD (70, 71).

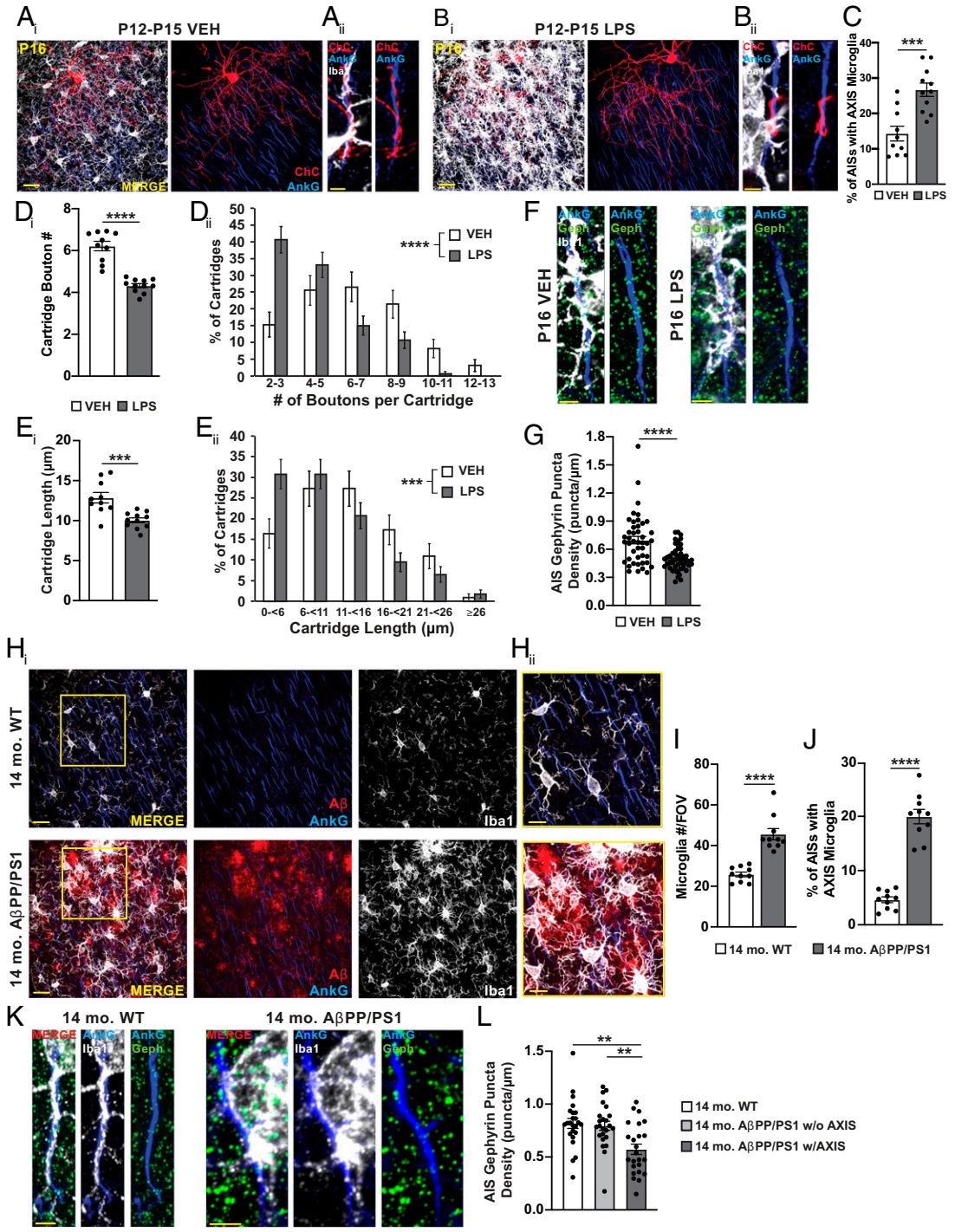

Fig. 6. Microglial activation perturbs neocortical ChC cartridge/bouton development and integrity. (A_i and B_i) Representative images of single RFP$^+$ ChCs, neighboring AnkG$^+$ AISs, and Iba1$^+$ microglia in L2/3 of the SSC from P16 *Nkx2.1-CreER;Ai9* mice administered LPS (B_i) or vehicle (A_i) once daily from P12 to P15. (Scale bars, 20 μm.) (A_{ii} and B_{ii}) Representative images of RFP$^+$ ChC cartridge–PyN AIS innervation with or without AXIS microglia contact in P16 *Nkx2.1-CreER;Ai9* mice under LPS (B_{ii}) or vehicle (A_{ii}) conditions. (Scale bars, 3 μm.) (*C*) Quantification of the percentage of AISs contacted by AXIS microglia in L2/3 of the SSC from P16 *Nkx2.1-CreER;Ai9* mice under LPS or vehicle conditions. (D_i and E_i) Quantification of the average number of boutons per ChC cartridge (D_i) and average length of ChC cartridges (E_i) innervating PyN AISs with AXIS microglia contact at P16 in the SSC of *Nkx2.1-CreER;Ai9* mice under LPS or vehicle conditions. (D_{ii} and E_{ii}) Frequency distribution histograms showing the percentage of ChC cartridges with bouton number per cartridge ranging from 2 to 13 boutons (D_{ii}) and cartridge length ranging from 0 to ≥26 μm (E_{ii}) with AXIS microglia contact at P16 under LPS or vehicle conditions. (*F*) Representative images of PyN AISs with AXIS microglia contact in L2/3 of the SSC from mice treated with LPS or vehicle from P12 to P15 and killed at P16. GABAergic synapses are visualized by immunostaining for gephyrin (Geph). (Scale bars, 3 μm.) (*G*) Quantification of average gephyrin puncta density at AISs with AXIS microglia contact at P16. (H_i) Representative images of L2/3 of the SSC from 14 mo. AβPP/PS1 and WT littermates immunostained for Aβ plaques (red), Iba1$^+$ microglia (white), and AnkG$^+$ AISs (blue). (Scale bars, 20 μm.) (H_{ii}) Magnified boxed *Insets* from H_i highlighting the close interactions between microglia, neurotoxic Aβ plaques, and AISs in AβPP/PS1, but not wild-type, animals. (Scale bars, 10 μm.) (*I* and *J*) Quantification of average microglia number per 200 μm × 200 μm FOV (*I*) and the percentage of AISs contacted by AXIS microglia (*J*) in 14 mo. AβPP/PS1 and wild-type littermates. (*K*) Representative images of PyN AISs with AXIS microglia contact in L2/3 of the SSC from 14 mo. AβPP/PS1 and wild-type littermates. GABAergic synapses are visualized by immunostaining for gephyrin (Geph). (Scale bars, 3 μm.) (*L*) Quantification of average gephyrin puncta density at AISs with or without AXIS microglia contact in 14 mo. AβPP/PS1 and WT littermates. For *C*, D_i, E_i, *G*, *I*, *J*, and *L*, data are mean ± SEM. For D_{ii} and E_{ii}, error bars indicate SEM for a multinomial distribution. $^{**}P < 0.01$, $^{***}P < 0.001$, $^{****}P < 0.0001$ (Student's *t* tests in *C*, D_i, E_i, *G*, *I*, and *J*; two-tailed Mann–Whitney *U* tests in D_{ii} and E_{ii}, one-way ANOVA with post hoc Tukey's multiple comparison test in *L*); *n* values and statistical information are listed in *SI Appendix*, Table S1.

Discussion

In this study, we identify a previously unrecognized synaptogenic role for microglia in the regulation of PyN axo-axonic synapse formation by ChCs, a unique type of GABAergic interneuron whose terminal axon cartridges selectively target the AIS (30). Such a discovery is supported by several lines of evidence. To begin, we show that: 1) a subset of microglia (referred to as AXIS microglia) closely interact with PyN AISs and ChC cartridges in L2/3 of the SSC, 2) the peak of such tripartite interactions coincides temporally with the period of most rapid postnatal ChC axonal development/synaptogenesis, and 3) similar to ChC/PyN AIS innervation, AXIS positioning of microglia is dependent on the unique AIS cytoskeleton (40). Next, we find that homeostatic AXIS microglia–AIS–ChC interactions in the postnatal developing SSC are associated with an increase in ChC cartridge length and bouton number and that depletion of microglia in the healthy brain impairs the proper formation/maintenance of ChC cartridges/boutons, as well as ChC/PyN AIS GABAergic synaptogenesis. Furthermore, we show that microglia–PyN AIS interactions rely on microglial $GABA_{B1}$Rs and that ablation of such receptors in microglia impacts proper ChC synaptogenesis. Finally, we demonstrate that microglial activation/dyshomeostasis under both LPS- and AD-induced neuroinflammatory states impairs ChC cartridge/bouton morphogenesis and synaptic connectivity at PyN AISs. Thus, our data identify microglia as key cellular players in the regulation of ChC/PyN axo-axonic synapse formation.

Our findings report a synaptogenic role for microglia in the regulation of inhibitory synapses in the postnatal developing brain. Such a function of microglia had hitherto only been demonstrated for excitatory synapses, with previous work demonstrating microglia-induced spine formation in the hippocampus and SSC (18, 21, 22). Studies on the role of microglia in modulating inhibitory synapses during postnatal development remain scarce. Only recently did work by Favuzzi et al. (29), which investigated the requirement of microglia in the pruning of inhibitory axo-somatic synapses, uncover a subset of GABA-receptive microglia that selectively interact with and remodel inhibitory axo-somatic synapses without impacting excitatory synapses during a critical window of mouse postnatal development. In light of these findings, it is conceivable that AXIS microglia represent a fraction of GABA-receptive microglia that contact GABAergic ChC terminals at PyN AISs (see further below).

Beyond this, our study sheds light on the mechanisms governing ChC/PyN axo-axonic synapse formation in the developing SSC. Synapse formation is a complex, multistep process, involving the recognition of specific postsynaptic targets by growing axons, the formation of initial contacts, and the assembly and maturation of pre- and postsynaptic specializations (1). To date, the only molecule known to regulate ChC/PyN AIS contact formation is L1CAM, which, via its interaction with the AIS-localized AnkG/βIV-spectrin cytoskeletal complex, directs ChC/PyN innervation selectively to the AIS of PyNs (40). Notably, while PyN L1CAM is essential for the establishment and maintenance of ChC/PyN AIS innervation, it is not sufficient for synapse formation, since ectopic expression of L1CAM in PyNs does not significantly increase AIS GABAergic synapse density (40). In contrast to this, AXIS microglia are not required for the establishment of ChC/PyN AIS contacts but instead regulate proper ChC cartridge/bouton morphogenesis and AIS synaptogenesis. Indeed, microglia depletion did not perturb ChC/PyN AIS innervation but significantly decreased the number of axo-axonic synapses at PyN AISs. Such findings reinforce the multistep nature of directed synapse formation with L1CAM being essential for initial ChC/PyN contact and AXIS microglia being required subsequently for proper ChC synapse development. In line with this, recent large-scale volumetric electron microscopy and functional imaging of ChC/PyN synaptic connectivity suggests that the number of ChC/PyN connections (i.e., innervation) and the number of synapses per connection (i.e., ChC boutons) are governed by different processes (72).

Concerning the involvement of different processes, our present data unveil a key role for microglial $GABA_{B1}$Rs in mediating microglia–PyN AIS interactions and ChC synaptogenesis. Combined with our previous findings on L1CAM (40), these data support a model in which L1CAM-mediated ChC/PyN AIS initial contact and subsequent GABAergic neurotransmission recruits microglia to the AIS of PyNs through microglial sensing of GABA via their expression of $GABA_{B1}$Rs. We do not exclude though that other mechanisms/players besides $GABA_{B1}$Rs may be involved in mediating AXIS microglia–PyN AIS–ChC interactions. For example, GABA-receptive microglia that contact ChC terminals at PyN AISs may express distinct CAMs that interact with partners selectively expressed at PyN AISs. In this regard, GABA-receptive microglia that sculpt axo-somatic synapses were reported to have higher levels of transcripts encoding various transmembrane proteins (29). It should also be noted that ChC cartridge/bouton development and synaptogenesis are dependent on ChC DOCK7/ErbB4-, FGF13-, and IgSF11-signaling (44–48), suggesting that these ChC-expressed molecules act in concert with AXIS microglia to regulate/coordinate different aspects of axo-axonic synapse assembly/maturation. In regards to AXIS microglia, one potential scenario is that GABA-recruited AXIS microglia release trophic factors/cytokines, such as brain-derived neurotrophic factor, interleukin-10 (IL-10), insulin-like growth factor, nerve growth factor, and basic fibroblast growth factor (FGF2), which locally promote ChC cartridge/bouton development and synaptogenesis (18, 67, 73–75). In support of this notion, microglial secretion of IL-10 in vitro was reported to promote the formation of inhibitory synapses in cultured neurons (67). In vivo, brain-derived neurotrophic factor release by microglia regulates learning-dependent spine formation and the expression levels of synapse-associated proteins (18). Future studies will be required to determine whether growth factors secreted by microglia regulate the establishment and maintenance of ChC cartridge/bouton synaptic structure and whether the release of other paracrine factors are involved.

The importance of homeostatic microglia in regulating proper ChC cartridge/bouton development and synaptogenesis is further highlighted by our findings that such processes are perturbed under neuroinflammatory and pathological conditions. Under acute LPS-induced neuroinflammatory conditions during early postnatal development, microglia activation precipitated an increase in AXIS microglia numbers and impeded ChC/PyN AIS synapse formation. Such a decrease in AIS synapses is not due to microglia-mediated phagocytosis of ChCs, as no significant engulfment of labeled ChC material by microglia in L2/3 of the SSC was observed. Instead, LPS-induced activation of microglia and subsequent alterations in their cytokine release profile (i.e., decrease in synaptogenic/trophic factors and increase in cytotoxic factors) likely hinders proper ChC cartridge/bouton morphogenesis and synapse formation during this critical period of ChC development (9, 65, 67). In

a similar vein, prolonged neuroinflammation, a hallmark of AD, induced microglia activation, increased AXIS microglia numbers, and facilitated the loss of GABAergic AIS synapses in the AβPP/PS1 mouse model of AD. Since ChC/PyN AIS synapse formation is largely complete by the onset of Aβ plaque deposition and resulting inflammation, it is probable that targeting of activated microglia to the AIS strips existing ChC/PyN axo-axonic synapses, especially since microglia-mediated stripping of PV synapses has already been reported to occur at the cell soma in response to neurological insult/injury (27, 28). Future work will be needed to fully elucidate the mechanisms underlying impaired ChC cartridge/bouton development and maintenance under pathological conditions.

In summary, our findings identify key roles for homeostatic microglia in the proper formation and maintenance of neocortical ChC cartridges/boutons and axo-axonic synapses. Accordingly, early postnatal disruption of proper microglia function, either via microglial depletion, $GABA_{B1}R$ removal, or immune activation, induced a significant decrease in PyN AIS GABAergic synaptic density. Microglia-mediated regulation of GABAergic axo-axonic synapses also extends into adulthood as chronic, AD-associated neuroinflammation and microglia activation induce the loss of inhibitory AIS synapses. Notably, the impact of such observed perturbations in ChC/PyN synapses is further compounded given that each AIS is typically innervated by three to four cartridges from three to four distinct ChCs (30, 43), whereas under our experimental conditions, analyses were performed on cartridges from single, labeled ChCs. Therefore, the effect of microglia dyshomeostasis (i.e., depletion or activation) on ChC cartridge/bouton structure and synaptic connectivity is in reality three to four times greater, likely impacting the physiological properties of ChCs and neocortical excitatory-inhibitory balance. In line with this, previous work investigating ChC-mediated inhibition of principal cells in the basolateral amygdala found that a minimum of 10 to 12 ChC synapses are required to prevent principal cell firing, providing further support for the importance of microglia in fine-tuning the number of boutons per ChC cartridge (76). Subtle changes in ChC bouton number have also been linked to aberrant behavioral phenotypes, since alterations in the density of ChC boutons in *Nkx2.1-CreER;erbb4*$^{-/-}$ animals, a model in which the schizophrenia-linked ErbB4 receptor tyrosine kinase is depleted from ChCs, induced schizophrenia-like behaviors (77). Thus, our findings, combined with the growing number of reports linking ChC structure/function to circuit activity and behavior, underscore the importance of tripartite ChC-PyN AIS-microglia communication in health and disease.

Materials and Methods

Nkx2.1-CreER, *Rosa26-loxpSTOPloxp-TdTomato* (*Ai9*), $GABA_{B1}R^{fl/fl}$, *Cx3cr1-Cre*, *APPswe,PSEN1de9* mice were maintained and bred as previously described (29, 35, 40, 69). All animal procedures were performed following the guidelines of Cold Spring Harbor Laboratory's Animal Care and Use Committee. For plasmid construction, cell culture/transfection, Western blotting, pharmacology-based microglia depletion/activation, and in utero electroporation at embryonic day 15.5, standard procedures were applied, as previously described (17, 27, 40, 47) and detailed in *SI Appendix, SI Material and Methods*. Details on brain sectioning and immunohistochemistry (47), as well as image acquisition and data analysis using Zeiss confocal microscopy and GraphPad Prism 8 software, are also described in *SI Appendix*. All conditions/genotypes during data acquisition and analysis were blinded to the experimenter. Information on antibodies and RNAi-targeting sequences are also included in *SI Appendix*.

Data Availability. All data are included in the main text and *SI Appendix*.

ACKNOWLEDGMENTS. We thank members of the L.V.A. laboratory and L. Cheadle for helpful discussions and critical reading of the manuscript; J. Kinney and T. Ha for assistance with statistical analyses; M. Rasband for providing critical reagents; Z. J. Huang for providing *Nkx2.1-CreER* and *Ai9* mice; B. Bettler for providing $GABA_{B1}R^{fl/fl}$ mice; D. Schafer and R. Stanley for providing brains from *Csf1r* knockout and wild-type mice; and N. Tonks for providing brains from *APPswe,PSEN1de9* and wild-type mice. This work was supported by NIH Grants R01MH119819 and R01NS116897 (to L.V.A.) and NIH Fellowship F31MH117871 (to N.B.G.).

1. T. C. Südhof, Towards an understanding of synapse formation. *Neuron* **100**, 276–293 (2018).
2. D. L. Chao, L. Ma, K. Shen, Transient cell-cell interactions in neural circuit formation. *Nat. Rev. Neurosci.* **10**, 262–271 (2009).
3. M. R. Akins, T. Biederer, Cell-cell interactions in synaptogenesis. *Curr. Opin. Neurobiol.* **16**, 83–89 (2006).
4. J. B. Zuchero, B. A. Barres, Glia in mammalian development and disease. *Development* **142**, 3805–3809 (2015).
5. R. D. Fields, B. Stevens-Graham, New insights into neuron-glia communication. *Science* **298**, 556–562 (2002).
6. J. A. Stogsdill, C. Eroglu, The interplay between neurons and glia in synapse development and plasticity. *Curr. Opin. Neurobiol.* **42**, 1–8 (2017).
7. N. J. Allen, D. A. Lyons, Glia as architects of central nervous system formation and function. *Science* **362**, 181–185 (2018).
8. M. Prinz, S. Jung, J. Priller, Microglia biology: One century of evolving concepts. *Cell* **179**, 292–311 (2019).
9. S. Werneburg, P. A. Feinberg, K. M. Johnson, D. P. Schafer, A microglia-cytokine axis to modulate synaptic connectivity and function. *Curr. Opin. Neurobiol.* **47**, 138–145 (2017).
10. C. Cserép, B. Pósfai, Á. Dénes, Shaping neuronal fate: Functional heterogeneity of direct microglia-neuron interactions. *Neuron* **109**, 222–240 (2021).
11. U. B. Eyo, L. J. Wu, Microglia: Lifelong patrolling immune cells of the brain. *Prog. Neurobiol.* **179**, 101614 (2019).
12. Y. Wu, L. Dissing-Olesen, B. A. MacVicar, B. Stevens, Microglia: Dynamic mediators of synapse development and plasticity. *Trends Immunol.* **36**, 605–613 (2015).
13. P. Squarzoni *et al.*, Microglia modulate wiring of the embryonic forebrain. *Cell Rep.* **8**, 1271–1279 (2014).
14. D. P. Schafer *et al.*, Microglia sculpt postnatal neural circuits in an activity and complement-dependent manner. *Neuron* **74**, 691–705 (2012).
15. R. C. Paolicelli *et al.*, Synaptic pruning by microglia is necessary for normal brain development. *Science* **333**, 1456–1458 (2011).
16. C. J. Bohlen, B. A. Friedman, B. Dejanovic, M. Sheng, Microglia in brain development, homeostasis, and neurodegeneration. *Annu. Rev. Genet.* **53**, 263–288 (2019).
17. C. Wang *et al.*, Microglia mediate forgetting via complement-dependent synaptic elimination. *Science* **367**, 688–694 (2020).
18. C. N. Parkhurst *et al.*, Microglia promote learning-dependent synapse formation through brain-derived neurotrophic factor. *Cell* **155**, 1596–1609 (2013).
19. A. Badimon *et al.*, Negative feedback control of neuronal activity by microglia. *Nature* **586**, 417–423 (2020).
20. M. Andoh, R. Koyama, Microglia regulate synaptic development and plasticity. *Dev. Neurobiol.* **81**, 568–590 (2021).
21. A. Miyamoto *et al.*, Microglia contact induces synapse formation in developing somatosensory cortex. *Nat. Commun.* **7**, 12540 (2016).
22. L. Weinhard *et al.*, Microglia remodel synapses by presynaptic trogocytosis and spine head filopodia induction. *Nat. Commun.* **9**, 1228 (2018).
23. G. O. Sipe *et al.*, Microglial P2Y12 is necessary for synaptic plasticity in mouse visual cortex. *Nat. Commun.* **7**, 10905 (2016).
24. P. T. Nguyen *et al.*, Microglial remodeling of the extracellular matrix promotes synapse plasticity. *Cell* **182**, 388–403.e15 (2020).
25. R. Tremblay, S. Lee, B. Rudy, GABAergic interneurons in the neocortex: From cellular properties to circuits. *Neuron* **91**, 260–292 (2016).
26. C. Cserép *et al.*, Microglia monitor and protect neuronal function through specialized somatic purinergic junctions. *Science* **367**, 528–537 (2020).
27. Z. Chen *et al.*, Microglial displacement of inhibitory synapses provides neuroprotection in the adult brain. *Nat. Commun.* **5**, 4486 (2014).
28. Y. Wan *et al.*, Microglial displacement of GABAergic synapses is a protective event during complex febrile seizures. *Cell Rep.* **33**, 108346 (2020).
29. E. Favuzzi *et al.*, GABA-receptive microglia selectively sculpt developing inhibitory circuits. *Cell* **184**, 4048–4063.e32 (2021).
30. N. B. Gallo, A. Paul, L. Van Aelst, Shedding light on chandelier cell development, connectivity, and contribution to neural disorders. *Trends Neurosci.* **43**, 565–580 (2020).
31. A. Howard, G. Tamas, I. Soltesz, Lighting the chandelier: New vistas for axo-axonic cells. *Trends Neurosci.* **28**, 310–316 (2005).
32. M. Inan, S. A. Anderson, The chandelier cell, form and function. *Curr. Opin. Neurobiol.* **26**, 142–148 (2014).
33. A. R. Woodruff, S. A. Anderson, R. Yuste, The enigmatic function of chandelier cells. *Front. Neurosci.* **4**, 201 (2010).
34. M. Inan, J. Welagen, S. A. Anderson, Spatial and temporal bias in the mitotic origins of somatostatin- and parvalbumin-expressing interneuron subgroups and the chandelier subtype in the medial ganglionic eminence. *Cereb. Cortex* **22**, 820–827 (2012).
35. H. Taniguchi, J. Lu, Z. J. Huang, The spatial and temporal origin of chandelier cells in mouse neocortex. *Science* **339**, 70–74 (2013).

36. M. C. Inda, J. Defelipe, A. Muñoz, The distribution of chandelier cell axon terminals that express the GABA plasma membrane transporter GAT-1 in the human neocortex. *Cereb. Cortex* **17**, 2060–2071 (2007).
37. J. Lu *et al.*, Selective inhibitory control of pyramidal neuron ensembles and cortical subnetworks by chandelier cells. *Nat. Neurosci.* **20**, 1377–1383 (2017).
38. T. J. Viney *et al.*, Network state-dependent inhibition of identified hippocampal CA3 axo-axonic cells in vivo. *Nat. Neurosci.* **16**, 1802–1811 (2013).
39. A. R. Woodruff *et al.*, State-dependent function of neocortical chandelier cells. *J. Neurosci.* **31**, 17872–17886 (2011).
40. Y. Tai, N. B. Gallo, M. Wang, J. R. Yu, L. Van Aelst, Axo-axonic innervation of neocortical pyramidal neurons by GABAergic chandelier cells requires AnkyrinG-associated L1CAM. *Neuron* **102**, 358–372.e9 (2019).
41. A. Pan-Vazquez, W. Wefelmeyer, V. Gonzalez Sabater, G. Neves, J. Burrone, Activity-dependent plasticity of axo-axonic synapses at the axon initial segment. *Neuron* **106**, 265–276.e6 (2020).
42. A. Steinecke *et al.*, Neocortical chandelier cells developmentally shape axonal arbors through reorganization but establish subcellular synapse specificity without refinement. *eNeuro* **4**, ENEURO.0057-17.2017 (2017).
43. M. Inan *et al.*, Dense and overlapping innervation of pyramidal neurons by chandelier cells. *J. Neurosci.* **33**, 1907–1914 (2013).
44. P. Fazzari *et al.*, Control of cortical GABA circuitry development by Nrg1 and ErbB4 signalling. *Nature* **464**, 1376–1380 (2010).
45. I. Del Pino *et al.*, Erbb4 deletion from fast-spiking interneurons causes schizophrenia-like phenotypes. *Neuron* **79**, 1152–1168 (2013).
46. E. Favuzzi *et al.*, Distinct molecular programs regulate synapse specificity in cortical inhibitory circuits. *Science* **363**, 413–417 (2019).
47. Y. Tai, J. A. Janas, C. L. Wang, L. Van Aelst, Regulation of chandelier cell cartridge and bouton development via DOCK7-mediated ErbB4 activation. *Cell Rep.* **6**, 254–263 (2014).
48. Y. Hayano *et al.*, IgSF11 homophilic adhesion proteins promote layer-specific synaptic assembly of the cortical interneuron subtype. *Sci. Adv.* **7**, eabf1600 (2021).
49. C. Leterrier, The axon initial segment, 50 years later: A nexus for neuronal organization and function. *Curr. Top. Membr.* **77**, 185–233 (2016).
50. M. N. Rasband, The axon initial segment and the maintenance of neuronal polarity. *Nat. Rev. Neurosci.* **11**, 552–562 (2010).
51. K. Baalman *et al.*, Axon initial segment-associated microglia. *J. Neurosci.* **35**, 2283–2292 (2015).
52. Y. Ogawa *et al.*, Postsynaptic density-93 clusters Kv1 channels at axon initial segments independently of Caspr2. *J. Neurosci.* **28**, 5731–5739 (2008).
53. A. M. Jurga, M. Paleczna, K. Z. Kuter, Overview of general and discriminating markers of differential microglia phenotypes. *Front. Cell. Neurosci.* **14**, 198 (2020).
54. B. S. Wang *et al.*, Retinal and callosal activity-dependent chandelier cell elimination shapes binocularity in primary visual cortex. *Neuron* **109**, 502–515.e7 (2021).
55. M. R. Elmore *et al.*, Colony-stimulating factor 1 receptor signaling is necessary for microglia viability, unmasking a microglia progenitor cell in the adult brain. *Neuron* **82**, 380–397 (2014).
56. B. Erblich, L. Zhu, A. M. Etgen, K. Dobrenis, J. W. Pollard, Absence of colony stimulation factor-1 receptor results in loss of microglia, disrupted brain development and olfactory deficits. *PLoS One* **6**, e26317 (2011).
57. A. M. Fontainhas *et al.*, Microglial morphology and dynamic behavior is regulated by ionotropic glutamatergic and GABAergic neurotransmission. *PLoS One* **6**, e15973 (2011).
58. T. R. Hammond *et al.*, Single-cell RNA sequencing of microglia throughout the mouse lifespan and in the injured brain reveals complex cell-state changes. *Immunity* **50**, 253–271.e6 (2019).
59. S. A. Kuhn *et al.*, Microglia express GABA(B) receptors to modulate interleukin release. *Mol. Cell. Neurosci.* **25**, 312–322 (2004).
60. Q. Li *et al.*, Developmental heterogeneity of microglia and brain myeloid cells revealed by deep single-cell RNA sequencing. *Neuron* **101**, 207–223.e10 (2019).
61. O. Matcovitch-Natan *et al.*, Microglia development follows a stepwise program to regulate brain homeostasis. *Science* **353**, aad8670 (2016).
62. D. D. Wang, A. R. Kriegstein, Defining the role of GABA in cortical development. *J. Physiol.* **587**, 1873–1879 (2009).
63. W. C. Oh, S. Lutzu, P. E. Castillo, H. B. Kwon, De novo synaptogenesis induced by GABA in the developing mouse cortex. *Science* **353**, 1037–1040 (2016).
64. O. Butovsky, H. L. Weiner, Microglial signatures and their role in health and disease. *Nat. Rev. Neurosci.* **19**, 622–635 (2018).
65. M. Kitayama, M. Ueno, T. Itakura, T. Yamashita, Activated microglia inhibit axonal growth through RGMa. *PLoS One* **6**, e25234 (2011).
66. M. W. Salter, B. Stevens, Microglia emerge as central players in brain disease. *Nat. Med.* **23**, 1018–1027 (2017).
67. S. H. Lim *et al.*, Neuronal synapse formation induced by microglia and interleukin 10. *PLoS One* **8**, e81218 (2013).
68. F. Leng, P. Edison, Neuroinflammation and microglial activation in Alzheimer disease: Where do we go from here? *Nat. Rev. Neurol.* **17**, 157–172 (2021).
69. D. R. Borchelt *et al.*, Accelerated amyloid deposition in the brains of transgenic mice coexpressing mutant presenilin 1 and amyloid precursor proteins. *Neuron* **19**, 939–945 (1997).
70. E. Vico Varela, G. Etter, S. Williams, Excitatory-inhibitory imbalance in Alzheimer's disease and therapeutic significance. *Neurobiol. Dis.* **127**, 605–615 (2019).
71. D. Bi, L. Wen, Z. Wu, Y. Shen, GABAergic dysfunction in excitatory and inhibitory (E/I) imbalance drives the pathogenesis of Alzheimer's disease. *Alzheimers Dement.* **16**, 1312–1329 (2020).
72. C. M. Schneider-Mizell *et al.*, Structure and function of axo-axonic inhibition. *Elife* **10**, e73783 (2021).
73. M. Ueno *et al.*, Layer V cortical neurons require microglial support for survival during postnatal development. *Nat. Neurosci.* **16**, 543–551 (2013).
74. K. Nakajima *et al.*, Neurotrophin secretion from cultured microglia. *J. Neurosci. Res.* **65**, 322–331 (2001).
75. D. M. Araujo, C. W. Cotman, Basic FGF in astroglial, microglial, and neuronal cultures: Characterization of binding sites and modulation of release by lymphokines and trophic factors. *J. Neurosci.* **12**, 1668–1678 (1992).
76. J. M. Veres, G. A. Nagy, V. K. Vereczki, T. Andrási, N. Hájos, Strategically positioned inhibitory synapses of axo-axonic cells potently control principal neuron spiking in the basolateral amygdala. *J. Neurosci.* **34**, 16194–16206 (2014).
77. J. M. Yang *et al.*, erbb4 deficits in chandelier cells of the medial prefrontal cortex confer cognitive dysfunctions: Implications for schizophrenia. *Cereb. Cortex* **29**, 4334–4346 (2019).